

Research Paper

Quantitative MALDI Imaging of Spatial Distributions and Dynamic Changes of Tetrandrine in Multiple Organs of Rats

Weiwei Tang^{1,2*}, Jun Chen^{1,2*}, Jie Zhou^{1,2}, Junyue Ge^{1,2}, Ying Zhang^{1,2}, Ping Li^{1,2}, Bin Li^{1,2}

1. State Key Laboratory of Natural Medicines, China Pharmaceutical University, Nanjing, 210009, China

2. School of Traditional Chinese Pharmacy, China Pharmaceutical University, Nanjing, 211198, China

* These authors contributed equally.

 Corresponding authors: E-mail: liping2004@126.com (P. Li), binli@cpu.edu.cn (B. Li), China Pharmaceutical University, Nanjing, 210009, China. Phone: +86 (025) 83271382© Ivyspring International Publisher. This is an open access article distributed under the terms of the Creative Commons Attribution (CC BY-NC) license (<https://creativecommons.org/licenses/by-nc/4.0/>). See <http://ivyspring.com/terms> for full terms and conditions.

Received: 2018.10.04; Accepted: 2018.12.22; Published: 2019.01.25

Abstract

Detailed spatio-temporal information on drug distribution in organs is of paramount importance to assess drug clinically-relevant properties and potential side-effects. Matrix-assisted laser desorption/ionization mass spectrometry imaging (MALDI MSI) as a label-free and sensitive imaging modality provides an additional means of accurately visualizing drug and its metabolites distributions in tissue sections. However, technical limitations, complex physiochemical environment of surface and low abundance of target drugs make quantitative MALDI imaging of drug and its metabolites quite challenging.

Methods: In this study, an internal standard correction strategy was applied for quantitative MALDI imaging of tetrandrine in multiple organs of rats including lung, liver, kidney, spleen, and heart. The feasibility and reliability of the developed quantitative MSI method were validated by conventional liquid chromatography-tandem MS (LC-MS/MS) analysis, and the two methods showed a significant correlation.

Results: The quantitative MALDI imaging method met the requirements of specificity, sensitivity and linearity. Tissue-specific spatio-temporal distribution patterns of tetrandrine in different organs were revealed after intravenous administration in the rat. Moreover, demethylated metabolite was detected in liver tissues.

Conclusions: The current work illustrates that quantitative MALDI imaging provides an alternative means of accurately addressing the problem of drug and its metabolites distribution in tissues, complementary to traditional LC-MS/MS of tissue homogenates and whole-body autoradiography (WBA). Quantitative spatio-chemical information obtained here can improve our understanding of pharmacokinetics (PK), pharmacodynamics (PD), and potential transient toxicities of tetrandrine in organs, and possibly direct further optimization of drug properties to reduce drug-induced organ toxicity.

Key words: quantitative MALDI imaging, drug tissue distribution, tetrandrine, spatio-temporal heterogeneity of drug metabolism

Introduction

Accurately mapping tissue-specific distribution, concentration, time course of accumulation, elimination of drug and its metabolites in target or

clinically non-relevant tissues is essential for a detailed understanding of drug pharmacokinetics (PK) and pharmacodynamics (PD), as well as the

mechanism of drug action. If such spatial PK and PD information are available, we can answer the questions related to where drugs accumulate selectively in normal or pathological tissues, where drugs express desirable efficacy and undesirable toxicity in tissue-specific regions. It also provides significant complementary information for enhancing our understanding of activity and safety of drug and metabolites when a drug binds to a specific region of an organ. For example, rifampicin can penetrate the sites of tuberculosis and accumulate in necrotic caseum. In contrast, moxifloxacin cannot diffuse well in caseum, concordant with its failure to shorten therapy in recent clinical trials [1]. Nevertheless, the spatial distribution of drug and metabolites in organs/tissues is seldom known. In routine PK/PD studies, the most popular method used for qualitative and quantitative analysis of average drug concentration within tissues is liquid chromatography coupled to mass spectrometry (LC-MS). However, in LC-MS spatial information is sacrificed during tissue homogenization [2, 3]. Whole-body autoradiography (WBA) is considered a standard approach to map the spatial distribution of drugs attributed to its high sensitivity and quantitative nature [4]. However, WBA technique is unable to distinguish parent drug from its metabolites because only the radioactively-labeled compounds can be detected. Furthermore, the risk of radiolabel loss may occur in the metabolic process. Additionally, the synthesis of radioactively-labeled drug compounds is difficult, time-consuming, and quite expensive [5, 6].

The advent of MS-based imaging techniques provides an alternative approach for *in situ* monitoring the localization of a drug and its metabolites across tissue sections. Mass spectrometry imaging (MSI) technology has been widely used for the acquisition of spatial distribution information of endogenous chemical components in various specimens such as human, animal and plant tissues, as well as microbial samples [7-11]. Among multiple MSI techniques, matrix-assisted laser desorption/ionization (MALDI) MSI technology is the most popular MSI modality which provides the most comprehensive mass range from small metabolites to macromolecular proteins, high spatial resolution, high-speed and throughput measurement in contrast to 4-7 day exposure time required in acquiring WBA image [12-14].

Currently, application of MALDI MSI in drug research and development has attracted intense attention from the pharmaceutical industry. Drug compound and metabolite concentration measured in plasma often cannot accurately represent the levels present in tissues. For example, if a drug accumulates

heterogeneously within a target tissue with high localization in small sub-regions of the tissue, the organ-to-plasma concentration ratio may be perceived as blood contamination. This discrepancy may generate misinterpretation of the toxicological efficacy and mechanism of the drug [15]. Therefore, accurate and quantitative visualization of the spatial distribution of drugs or drug candidates is necessary for drug development and property optimization of drug-like compounds.

MALDI imaging that makes it superior to conventional optical imaging techniques lie in its label-free, unparalleled chemical information and spatially resolved detection. However, by its nature, absolute quantitation using MALDI MS encounters many challenges such as ion suppression, signal variations and organic matrix interference in the mass range below m/z 500. Recently, an active area in MALDI imaging of drug compounds is to develop specific quantitative MALDI imaging solutions to minimize or overcome these disadvantages. For example, many strategies have been developed for the improvement of the quantitative capability of MALDI imaging by various MSI data normalization methods [16-19], different calibration routines [20, 21], as well as quantitative software [22, 23].

Tetrandrine is a bisbenzylisoquinoline alkaloid extracted from *Stephania tetrandra* S. Moor. Pharmacological and clinical studies have proved its strong bioactivities including anti-silicosis [24], anti-cardiac hypertrophy [25] and anti-cancer activity [26]. With LC-MS/MS method, the PK profiles of tetrandrine and its average concentration in organs have been investigated after various routes of administration, which provide critical information for the discovery of optimal dose and route of administration [27]. However, the spatial distribution of tetrandrine in tissues has not been entirely and accurately delineated. Previous studies further indicated that tetrandrine or its metabolites may cause slight or transient toxicity in the target organs such as pulmonary [28], hepatic [29, 30] and renal toxicities [31]. Therefore, in present work, a quantitative MALDI MS imaging method was developed, evaluated and applied to spatially resolved quantitation of tetrandrine distribution in multiple organs of rats. For the first time, spatial distribution pattern and dynamic changes of tetrandrine were comprehensively studied in rat lung, liver, kidney, spleen and heart. Quantitative spatio-chemical information obtained here can improve our understanding of the ADME characteristics of tetrandrine in organs, and possibly direct further optimization of drug compound properties to reduce drug-induced organ toxicity.

Materials and Methods

Materials

Tetrandrine (purity >98%) was obtained from MUST Bio-Technology (Chengdu, China). Fangchinoline and daurisorline (purity >98%) were purchased from Yuanye Biotech (Shanghai, China). HPLC-grade acetonitrile and methanol were purchased from Merck (Darmstadt, Germany). Deionized water was prepared by a Milli-Q water purification system (Millipore, Billerica, MA, USA). The MALDI matrices 2,5-dihydroxybenzoic acid (DHB), and α -cyano-4-hydroxycinnamic acid (CHCA) were purchased from Sigma-Aldrich (St. Louis, MO, USA).

Animal study and sample collection

Male 8-week-old Sprague-Dawley rats were purchased from Qinglongshan Animal Center (License: SCXK 2014-0001; Nanjing, China) and kept in an environmentally controlled breeding room for at least one week before the experiment. Animal experiments were carried out in accordance with the Guidelines for Animal Experimentation of China Pharmaceutical University (Nanjing, China), and approved by the Animal Ethics Committee of this institution. After 12 h of fasting, rats were administered intravenously (*i.v.*) at a single dose of 30 mg kg⁻¹ tetrandrine. Blood, lung, liver, kidney, spleen, and heart samples were collected at 0, 10, 30, 60, 120 and 240 min after *i.v.* administration. Each heparinized blood sample was immediately centrifuged at 4,900 $\times g$ for 5 min and the supernatant of plasma was transferred to a clean tube. The organs were surgically dissected, washed with ice-cold saline, and stored at -80 °C until use.

Sample preparation for LC-MS/MS analysis

Plasma was processed following a routine laboratory procedure. 500 μ L of precipitation reagent acetonitrile containing 50 ng mL⁻¹ daurisorline (internal standard) was added to 100 μ L plasma. The vials were vortexed for 3 min, and centrifuged at 16,200 $\times g$ for 10 min. The supernatant was injected to LC-MS/MS system for analysis. Organ samples for LC-MS/MS analysis were processed as follows: samples were accurately weighed and homogenized in 1 mL of saline solution (1:5, W/V) using an automatic homogenizer. 100 μ L of tissue homogenate was mixed with 500 μ L of precipitation reagent acetonitrile containing 50 ng mL⁻¹ of IS, and the subsequent processes were in concordance with plasma samples.

Sample preparation for MALDI MS imaging

Multiple 12 μ m thick serial sections were obtained at -20 °C using a cryomicrotome (Leica,

Germany), and thaw-mounted onto indium tin oxide (ITO)-coated glass slides. Prior to matrix coating, the tissue sections were placed in a vacuum desiccator to dehydrate for 10 min at room temperature. Home-built electric field-assisted matrix coating setup was used to homogeneously deposit matrix onto tissue sections [32]. Briefly, 100 μ L of 60 mg mL⁻¹ DHB matrix solution containing 200 pg μ L⁻¹ IS was deposited onto tissue sections at a flow rate of 1 mL h⁻¹. The automatic sprayer parameters for matrix coating were as follows: sheath gas flow, 0.3 MPa; heated temperature, 100 °C; reciprocating motion speed, 0.17 m s⁻¹; high voltage between the sprayer needle and ITO slide, 6 kV; the distance between the spray needle and ITO slide, 12 cm.

LC-MS/MS analysis

LC-MS/MS experiments were performed using an Agilent 6460 QQQ mass spectrometer connected to an Agilent 1260 series UHPLC system (Agilent Technologies, CA, USA). Analytes were separated on an Agilent XDB C₁₈ column (4.6 mm \times 100 mm, 1.8 μ m) preceded by a guard column (5 mm \times 4.6 mm, 1.8 μ m, Agilent Eclipse XDB-C₁₈) at 30 °C. Mobile phase A was water containing 0.1% formic acid (V/V) and phase B was acetonitrile. The flow rate of the mobile phase was 0.4 mL min⁻¹. The gradient program was conducted as follows: 0.0-1.5 min, 10% B; 1.5-5 min, 10%-90% B; 5-6 min, 90%-10% B. The injection volume was 1 μ L. The mass spectrometer was operated in positive ion mode and the electrospray ionization (ESI) source parameters were as follows: drying gas temperature, 350 °C; drying gas flow, 10.0 L min⁻¹; sheath gas temperature, 300 °C; sheath gas flow, 11 L min⁻¹; nebulizer pressure, 45 psi; capillary voltage, 3.5 kV. Quantification analysis was performed in multiple-reaction monitoring (MRM) mode with the ion transitions of *m/z* 623.3 to 381.3 for tetrandrine and *m/z* 611.3 to 192.3 for IS, respectively. The collision energy was set to 45 eV for both parent drug and IS. Data collection and processing were conducted with MassHunter Workstation 05.00 (Agilent Technologies, USA).

MALDI MS imaging

MALDI MS imaging was performed using an UltrafleXtreme MALDI TOF/TOF MS (Bruker Daltonics, USA) with a frequency tripled Nd:YAG solid-state laser (λ = 355nm). The laser was set to the 'Ultra' footprint setting at an \sim 100 μ m diameter. Mass spectrometer calibration was performed using DHB matrix ions and a Peptide Calibration Standard Kit II (Bruker Daltonics). Tissue sections were analyzed in positive reflectron ion mode with 100 laser shots fired at 1000 Hz and imaged with a 100 μ m or 400 μ m laser

step size. MSI data was analyzed using flexAnalysis 3.4 and flexImaging 4.1 (Bruker Daltonics). Additionally, accurate mass measurement and tandem MS analysis of tetrandrine metabolite were performed on a 9.4T solariX™ Fourier transform ion cyclotron resonance (FT-ICR) mass spectrometer equipped with a dual MALDI and ESI source (Bruker Daltonics, USA). Data were analyzed using Data Analysis 4.0 (Bruker). For 3D MALDI imaging of kidney, 7 kidney sections, in 300 µm steps throughout the half tissue volume, were subjected to MALDI MSI analysis. The data for all 7 sections were imported into the software SCiLS Lab version 2016b (SCiLS, Bremen, Germany) to reconstruct the original relations between the sections.

Quantitative and statistical analysis of MALDI MSI data

Data was exported as an imzML file from flexImaging and imported into MSiReader v1.00 [23]. For standard curve generation and quantitation, the *m/z* intensity data for each region of interest (ROI) was exported to Excel using the MSiReader ROI tool ("sum of window" over 0.15 Da). The data for quantitative imaging was normalized to the signal from the IS *via* pixel by pixel (see Supporting Information-Peak Normalization). Statistical analyses were performed using GraphPad Prism 5.0 (San Diego, CA, USA).

Results and Discussion

Optimization of parameters for quantitative MALDI MSI

Since the choice of the matrix is crucial in MALDI MS imaging experiment, frequently used matrices including DHB and CHCA were evaluated and compared with the detection of tetrandrine spotted on blank tissues. As shown in **Figure S1**, the protonated ion of tetrandrine at *m/z* 623.3 was observed in mass spectra when coated with DHB or CHCA. However, DHB matrix produced higher signal intensity for tetrandrine than CHCA. Additionally, potassium and sodium adduct ions of tetrandrine were rarely detected with both matrices. Therefore, DHB was selected for analyzing the rat tissue sections. Moreover, homogeneous deposition of MALDI matrix onto tissue surface is essential to obtain the high quality MALDI MSI data. For example, sublimation and commercial automatic sprayers such as SunCollect™ or TM-Sprayer™ are widely used to evenly apply matrix. In this work, a homemade electronic-assisted automatic sprayer system was applied to ensure a homogeneous and reproducible deposition of DHB matrix.

To achieve reliable quantitative MALDI MSI results, the internal standard (IS) was incorporated in the matrix solution to compensate signal variation resulting from the complex surface properties and varied matrix-analyte interaction [33, 34]. Fangchinoline and daurisolone were considered as IS candidates due to their similar structures to tetrandrine. As shown in **Figure S2**, protonated ions of two IS are the major adducted ions detected with DHB, showing the similar ionization pattern to tetrandrine. However, fangchinoline (*m/z* 609.3) was excluded because it might interfere with the detection of tetrandrine-demethylated metabolite ions *m/z* 609.3 [35]. Therefore, daurisolone was selected as the internal standard. Additionally, considering that the possible interference peaks arose from different organs may affect the detection of tetrandrine and IS. Standards were spotted on five tissues and no interference peaks were observed by comparing with the blank tissues (**Figure S3**).

Validation of quantitative MALDI MSI

To further investigate the correction ability of the IS for the accurate quantitative MALDI MS imaging, linear regression analysis was performed on standard curves generated with IS-based normalization method. 0.1 µL of standard solutions of tetrandrine with concentrations ranging from 5 to 200 ng µL⁻¹ were spotted on blank rat tissue sections, and the mixture of DHB and IS was homogeneously sprayed on the tissue sections.

The standard curve was generated for tetrandrine by plotting average ion intensities of mass spectra in defined ROI as a function of the quantities of standard spotted on different tissue sections (**Figure 1**). As shown in **Figure 1** and **Table S1**, non-normalized data yielded the lower linear correlation coefficients ($R^2=0.9104-0.9974$), whereas the higher correlation coefficients were obtained using the IS-based normalization ($R^2=0.9924-0.9991$). Meanwhile, the lower limit of quantification (LLOQ) was investigated by analyzing standards spotted on different tissues. The LLOQ was 3 ng µL⁻¹ in lung tissue, and 4 ng µL⁻¹ in liver, kidney, spleen and heart tissues (**Figure S5** and **Table S1**), and signal-to-noise ratios (S/N) were all above 10 with acceptable precision and accuracy. Furthermore, correlation of the quantitative results obtained by MALDI MSI and LC-MS/MS was performed to validate the accuracy of the developed quantitative MALDI MS imaging method. The absolute concentrations of tetrandrine in each tissue were calculated by using calibration curves generated by quantitative MALDI MSI (**Figure 1**) and LC-MS/MS experiments (**Figure S6**), respectively. As shown in **Figure 2**, the concentration

of tetrandrine obtained by MALDI MSI correlated strongly with the average concentrations in different organs obtained by LC-MS/MS, with a correlation coefficient of $R^2=0.8942$ and $p=0.0151$ for lung, $R^2=0.7786$ and $p=0.0476$ for liver, $R^2=0.8281$ and $p=0.0320$ for kidney, $R^2=0.9229$ and $p=0.0093$ for spleen and $R^2=0.9412$ and $p=0.0062$ for heart.

Additionally, the temporal change of tetrandrine in tissues also show good agreement with the results obtained by two methods. The correlation analysis of these two results suggested that the IS-based normalization method is reliable for quantitatively exploring the changes of tetrandrine in multiple rat organs with MALDI MSI.

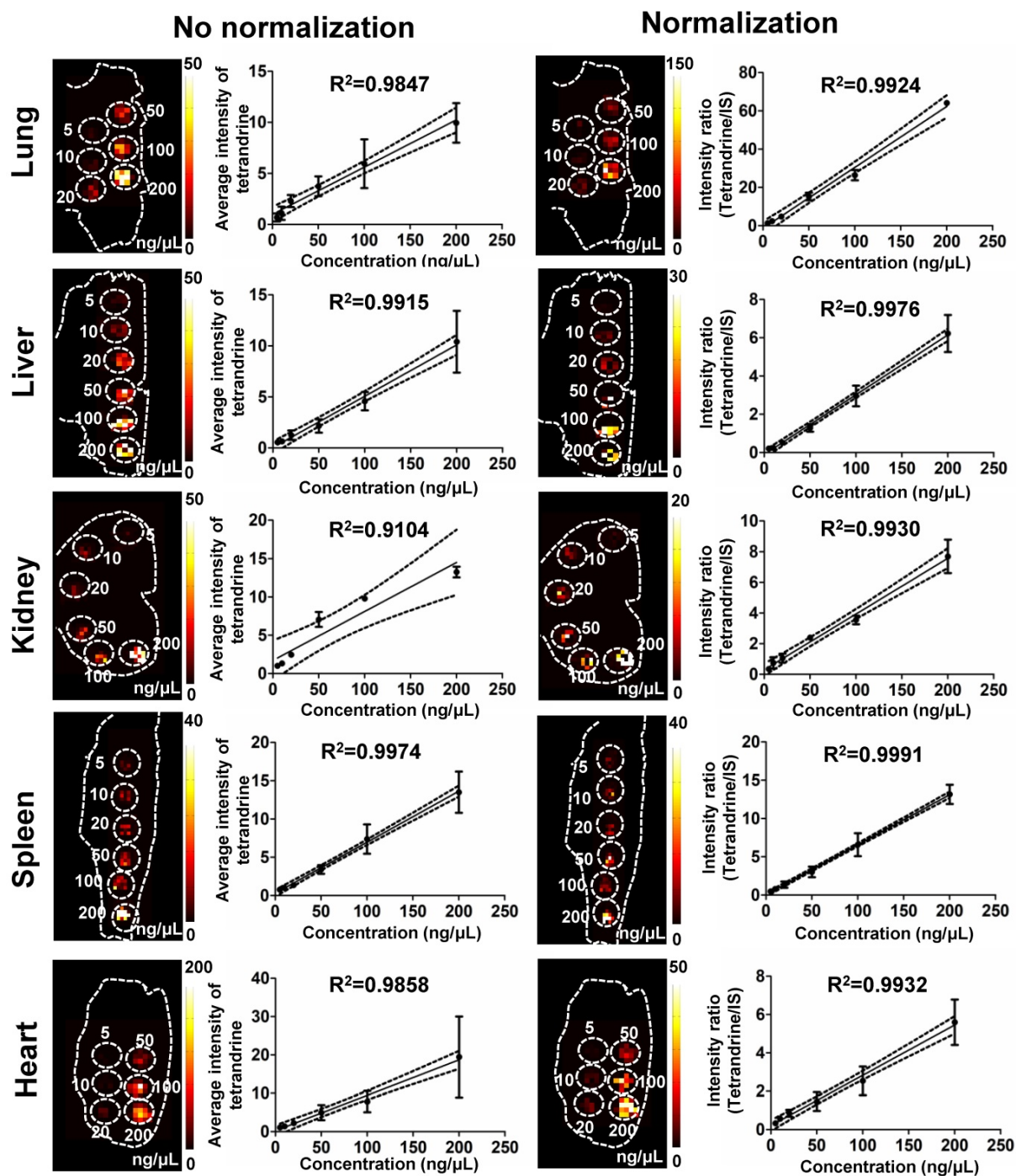


Figure 1. Comparison of linearity of calibration curves of tetrandrine standards obtained by using non-normalization and IS-based normalization. Calibration curves generated by plotting the intensity values of $[\text{tetrandrine}+\text{H}]^+$ and $[\text{tetrandrine}+\text{H}]^+ / [\text{IS}+\text{H}]^+$ as a function of the concentrations of tetrandrine spotted onto tissue sections. Ion images of different tissue sections with circles indicating places where tetrandrine standard solutions were applied in the range of 5–200 $\text{ng}/\mu\text{L}$ and coated with the DHB matrix (60 mg/mL) containing IS (200 $\text{pg}/\mu\text{L}$). Unnormalized and normalized ion images represent the distribution of $[\text{tetrandrine}+\text{H}]^+$ across the section surfaces. The calibration results were expressed as the mean \pm SD from three independent experiments.

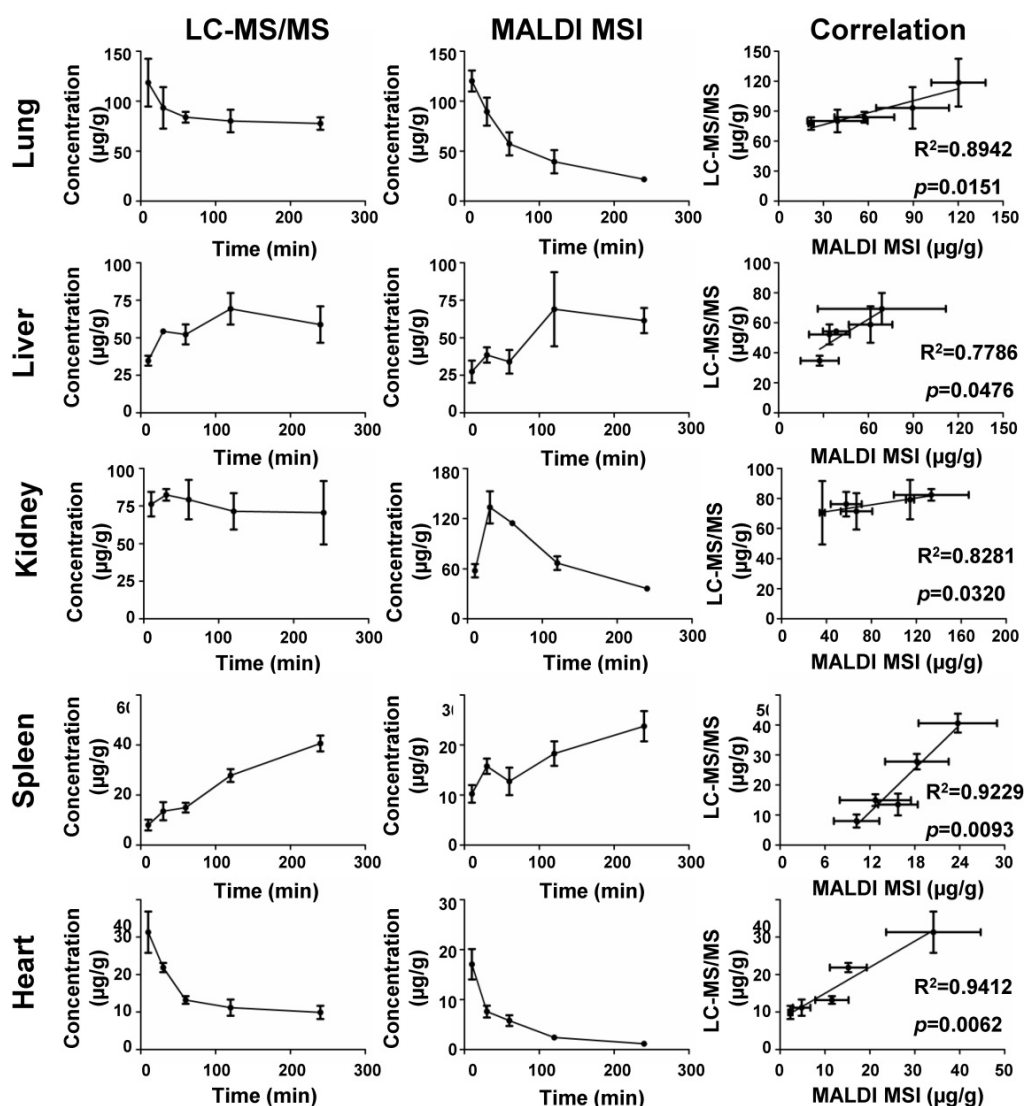


Figure 2. Correlation of the amount of tetrandrine at different time points determined by MALDI MSI and LC-MS/MS results from different tissues. The results were expressed as the mean \pm SD from three independent animals.

In previous studies, Chumbley et al. mentioned that premixing the IS with the matrix led to the underestimation of the actual amount of drug in tissues [34]. In our work, the quantitative results obtained by MALDI MSI and LC-MS/MS measurements were compared in different tissues. As shown in **Figure S4**, in liver and heart, measured concentrations with MALDI MSI and LC-MS/MS did not show a large difference. However, in lung and spleen, tetrandrine concentrations measured by MALDI MSI were lower than those by LC-MS/MS. Conversely, tetrandrine concentrations in kidney measured by MALDI MSI were higher than those by LC-MS/MS. The standard pre-mixed approach can therefore not correct all possible interferences originated from the heterogeneity of tissues and ion suppressions. However, it is an optional correction approach for obtaining accurate quantitative MALDI imaging results. As shown in **Figure 2**, the amount of

tetrandrine obtained by MALDI MSI correlated well with the average concentrations in different organs obtained by LC-MS/MS.

Spatio-temporal distribution of tetrandrine in different rat tissues

The detailed spatio-temporal information on tetrandrine distribution in organs has not been reported previously compared to its pharmacological, PK and PD studies. In this work, a fully validated quantitative MALDI MS imaging method was applied to investigate the spatio-temporal distribution of tetrandrine and its metabolites in lung, liver, kidney, spleen, and heart.

Lung

Tetrandrine has been used for the treatment of pulmonary diseases, such as silicosis [24], asthma [36] and pulmonary hypertension [37]. Therefore,

monitoring its distribution and dynamic changes in lung tissues were first conducted. After *i.v.* administration of tetrandrine, lung sections and homogenates were collected parallelly for quantitative MALDI MSI and LC-MS/MS analysis. The identity of the drug was verified by *in situ* accurate mass and tandem MS measurements. For m/z 623.3116, the ion formula was calculated as $[C_{38}H_{42}N_2O_6+H]^+$ with -0.06 ppm mass accuracy, and the identity of tetrandrine was further confirmed by characteristic fragment peaks at m/z 592.2701 and 381.1815 obtained on dosed lung tissue sections by MALDI CID-FT-ICR MS/MS (Figure 3A).

As shown in Figure 2 and Figure S8A, overall lung tissue time-concentration curve (TCC) shows a similar trend as measured blood TCC. After *i.v.* administration, the drug rapidly transfers from the blood into lung tissues, reaching maximum concentration (T_{max}) in 10 min. Subsequently, tissue and plasma concentrations rapidly decline from peak concentrations (Figure 3B) consistent with previous data [38]. As shown by H&E staining, rat left lung tissue contains three basic regions: apical region, central region and basal region (Figure 3C). Overall, tetrandrine displayed a non-uniform distribution in three regions. In ion images, the intensities of tetrandrine ion are highest in the basal region,

indicating a higher accumulation of the drug in this area compared to the apical and central region. From the aspect of spatio-temporal distribution, tetrandrine elimination showed intra-tissue variation, and a faster elimination rate was observed in the apical and central region particularly evident at 60 min and 120 min time-points. One possible reason for the temporal-spatial dynamic change can be attributed to the lung heterogeneities such as different regional blood flow. The basal region of lung receives higher levels of perfusion due to the gravity effect. Consequently, the lung apical and central region display the poor perfusion [39]. Therefore, blood flow gradient drives more tetrandrine to basal region. Additionally, the drug was less observed in the lung airways compared to surrounding regions, indicating that *i.v.* administration cannot deliver the tetrandrine to lung airways in contrast to inhaled administration. To confirm the heterogeneous distribution of tetrandrine in lung tissues, we performed LC-MS/MS analysis of homogenates on different parts of the lung tissues (Figure 3C) and MALDI imaging at $100\ \mu\text{m}$ (Figure S7). Samples collected at 60 min after drug administration were selected as representative tissue samples for validation. Tissue section ($150\ \mu\text{m}$ thickness) was dissected as shown in Figure 3C, and the segment 1 and 2 were extracted for LC-MS/MS

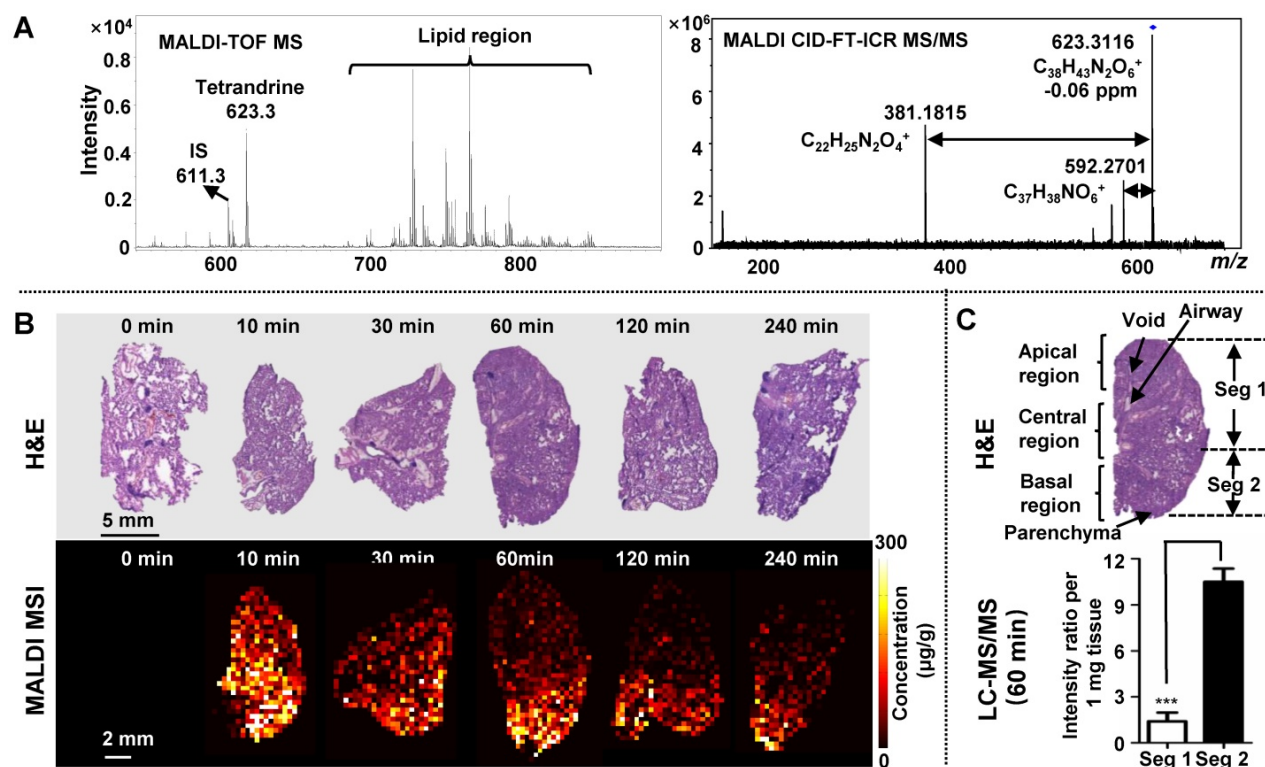


Figure 3. MALDI MS imaging analysis of the tetrandrine distribution in lung tissues after *i.v.* administration at single doses of $30\ \text{mg}\ \text{kg}^{-1}$ tetrandrine. (A) Single-pixel MALDI TOF MS spectrum of tetrandrine, IS and lipids from lung tissue (left) and MALDI CID-FT-ICR MS/MS spectrum of tetrandrine (right). (B) H&E staining of tissue sections obtained at different time points (top) and MALDI images represent the spatio-temporal distribution of tetrandrine across lung tissue sections (bottom). (C) Comparison of tetrandrine in lung tissues between the Seg 1 and 2 quantified using LC-MS/MS. The results were expressed as the mean \pm SD from three independent animals. Student's t-test was used for comparing two groups. *, significantly different between two groups at $p < 0.05$; **, $p < 0.01$ and ***, $p < 0.001$; n.s. as no significant difference between two groups.

analysis, respectively. Results of LC-MS/MS show that the relative amount of tetrandrine was significantly higher in the basal region compared to the central and apical region. Additionally, the ion images obtained at 400 μm (Figure 3B) and 100 μm (Figure S7) show a similar distribution pattern, confirming the heterogeneous distribution pattern of tetrandrine in lung tissues. Previous study indicated that tetrandrine was relatively non-toxic up to 90 mg kg^{-1} body weight [40]. However, in lung tissues, quinone methide metabolite of tetrandrine could have been generated from the metabolism by CYP3A4 and CYP3A5, which possibly lead to pulmonary toxicity [28, 41]. Therefore, the relatively more amount of tetrandrine in the basal region may result in the accumulation of toxic quinone methide metabolites, which possibly induce region-specific pulmonary toxicity.

Liver

Liver is a critical organ responsible for drug metabolism in which drug is mainly converted to water-soluble compounds facilitating excretion of the drug from the kidney [42]. As shown in Figure 2, MALDI MSI and LC-MS/MS measurements of TCC reveal a similar trend of tetrandrine in liver, reaching T_{max} in 120 min [38]. One possible metabolite

demethylated tetrandrine was detected and its identity was confirmed by accurate mass and tandem MS. As shown in Figure 4A, m/z 609.2965 calculated as $[\text{C}_{37}\text{H}_{40}\text{N}_2\text{O}_6+\text{H}]^+$ with -0.96 ppm mass accuracy is proposed as a demethylated metabolite of tetrandrine. The identity of metabolite was further confirmed by characteristic fragment peaks at m/z 578.2532 and 367.1659 (Figure S8B), consistent with literature data [35]. It should be noted that tetrandrine has several methoxy substitutions at various positions, and therefore a group of isomeric demethylated metabolites may be generated [35]. Due to the lack of LC separation and no characteristic fragments obtained by *in situ* tandem MS, it is unable to distinguish isomeric demethylated tetrandrine metabolites such as the O-demethylated or N-demethylated tetrandrine. Moreover, besides tetrandrine metabolite m/z 609.2965, no other tetrandrine metabolites such as glucuronide conjugates were detected in current work. Development of matrix-free LDI methods may provide an alternative approach to improve drug/metabolite detection from complex tissues [43-45].

In Figure 4B, tetrandrine shows relatively homogeneous distribution pattern in liver. To confirm this distribution pattern, we performed LC-MS/MS

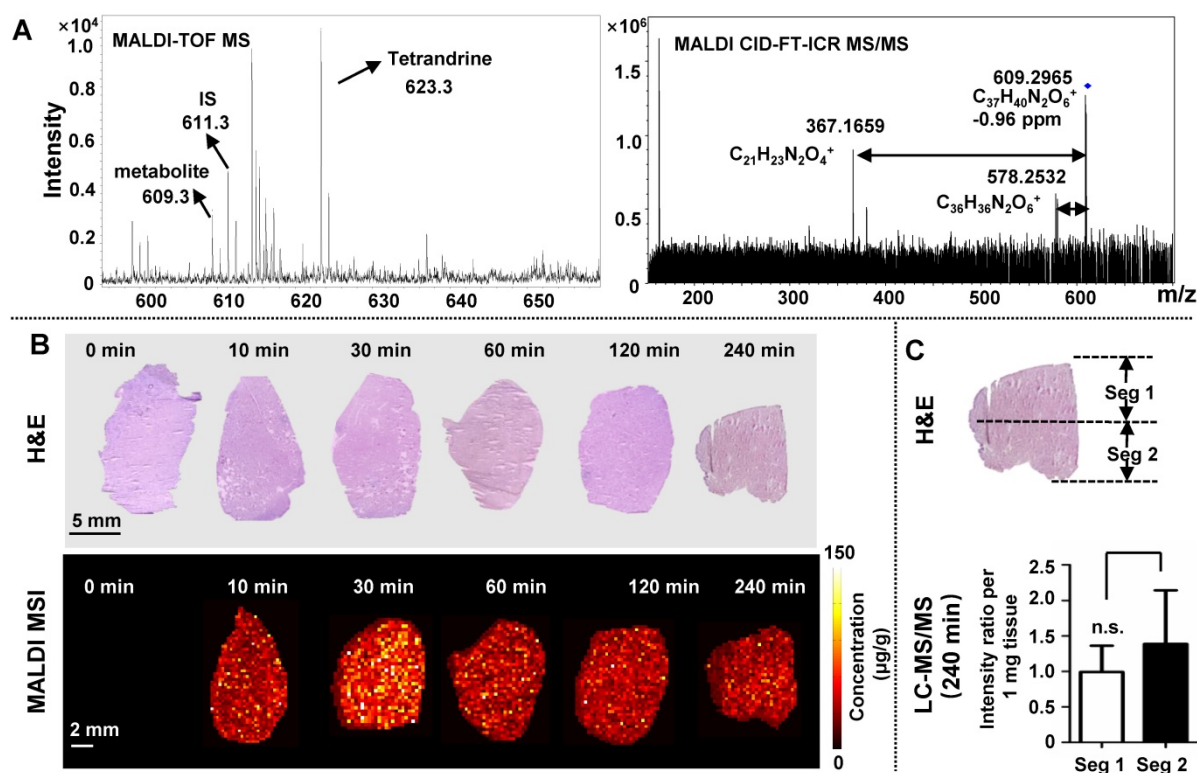


Figure 4. MALDI MS imaging analysis of the tetrandrine distribution in liver tissues after *i.v.* administration. (A) Single-pixel MALDI TOF MS spectrum of tetrandrine, one tetrandrine metabolite and IS from lung tissue (left) and MALDI CID-FT-ICR MS/MS spectrum of tetrandrine metabolite (right). (B) H&E staining of tissue sections obtained at different time points (top) and MALDI images represent the spatio-temporal distribution of tetrandrine across liver tissue sections (bottom). (C) Comparison of tetrandrine in liver tissues between the Seg 1 and 2 quantified using LC-MS/MS. The results were expressed as the mean \pm SD from three independent animals. Student's t-test was used for comparing two groups. *, significantly different between two groups at $p < 0.05$; **, $p < 0.01$ and ***, $p < 0.001$; n.s. as no significant difference between two groups.

analysis of homogenates of different parts of liver tissues (Figure 4C) and MALDI imaging at 100 μm (Figure S7). Samples collected at 240 min after drug administration were selected as representative tissue samples for validation. Statistical analyses of the relative amount of tetrandrine in segment 1 and 2 showed that no significant difference was observed in apical and bottom region of liver sections. Additionally, the ion images obtained at 400 μm (Figure 4B) and 100 μm (Figure S7) show similar distribution pattern, confirming the relatively homogenous distribution pattern of tetrandrine in liver tissues.

Previous studies demonstrated that dimethylated tetrandrine shares similar pharmacological activities with the parent drug tetrandrine [46-48]. In this work, the demethylated tetrandrine is generated following the exposure of tetrandrine and reaches the maximum concentration 4 h after injection (Figure S8C). Therefore, accumulation of demethylated tetrandrine in liver may enhance the efficacy of the parent drug. On the other hand, the possible increased risk of liver injury may occur, since demethylated metabolite of tetrandrine was reported to reduce the hepatocyte viability [30].

Kidney

Kidney is a highly heterogeneous organ responsible for drug excretion. Overall MALDI MSI and LC-MS/MS measurements of TCC show a similar

trend of tetrandrine in kidney, reaching T_{max} in 30 min (Figure 2). Tetrandrine is observed in renal tissue 10 min after administration and excreted rapidly *via* the renal system. The rat kidney consists of several tissue zones including cortex, medulla, pelvis, and hilum. In Figure 5A, the heterogeneous spatio-temporal distribution of tetrandrine was observed in kidney, which was mainly distributed in pelvis, medulla, and cortex. At 10 min, the tetrandrine was mainly detected in cortex and hilum. Subsequently, the distribution of tetrandrine spread to medulla and pelvis region. At 60 min, tetrandrine was mainly confined in the cortex and hilum regions. Furthermore, samples collected at 60 min were selected for 3-dimensional (3D) imaging considering that 3D cellular organization is typical of living organs. 3D MALDI imaging was performed by serial sectioning of dosed kidney sample followed by 2D imaging analysis of each section. In Figure 5B, seven slices of kidney were sectioned from the outside to the middle of the half kidney with 300 μm distance between the sister sections, and orderly displayed from outside to central part. The rightmost 3D volume reconstructed ion image confirmed that tetrandrine was mainly distributed in the cortex of kidney at 60 min. The MS imaging results suggest that the tetrandrine remained in renal cortex at a relatively high level may cause potential renal injury [31, 40].

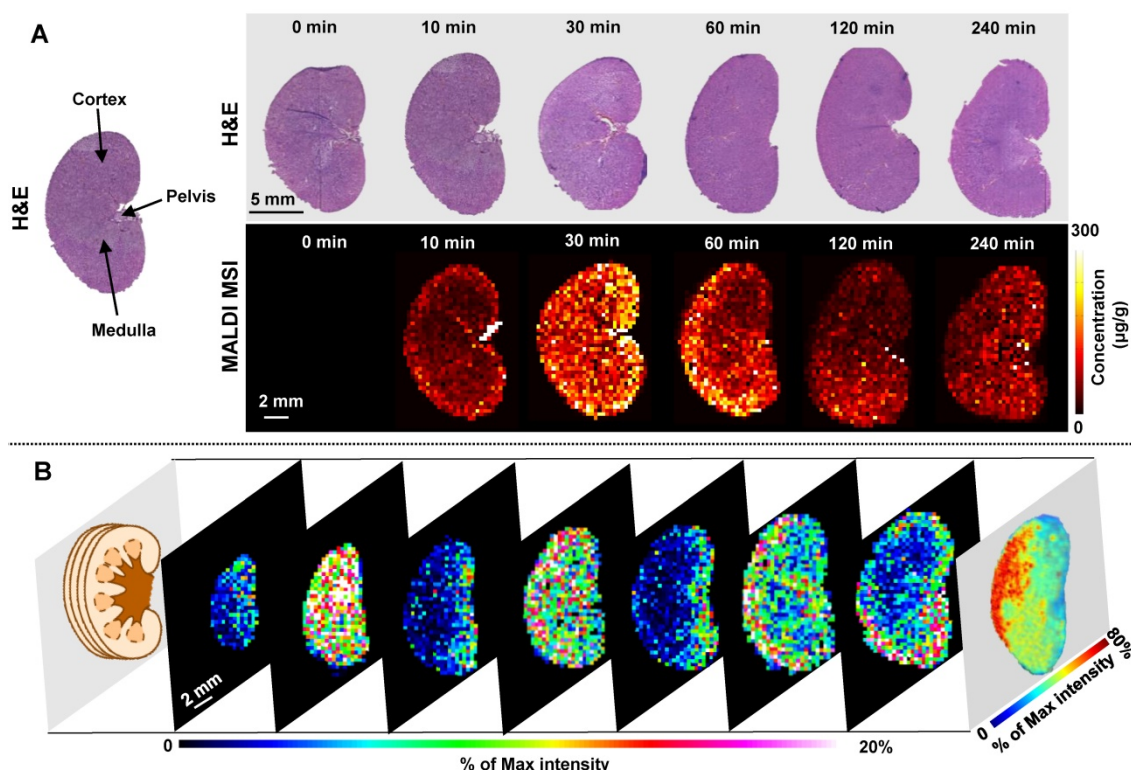


Figure 5. MALDI MS imaging analysis of the tetrandrine distribution in kidney tissues after *i.v.* administration. **(A)** H&E staining of tissue sections obtained at different time points (top) and MALDI images represent the spatio-temporal distribution of tetrandrine across kidney tissue sections (bottom). **(B)** 3D MALDI MS imaging of tetrandrine in kidney (60 min post-dose).

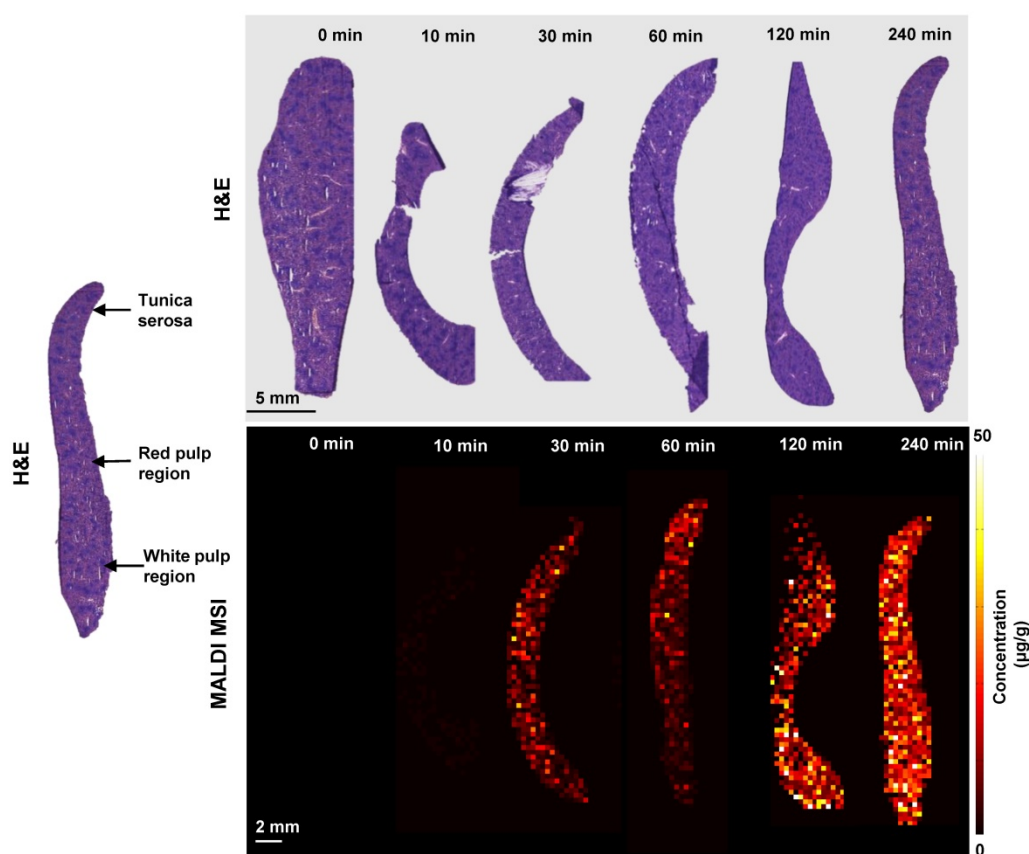


Figure 6. MALDI MS imaging analysis of the tetrandrine distribution in spleen tissues after *i.v.* administration. H&E staining of tissue sections obtained at different time points (top) and MALDI images represent the spatio-temporal distribution of tetrandrine across spleen tissue sections (bottom).

Spleen

Spleen as the largest secondary lymphoid organ, playing a significant role in erythrocytes and the immune system. However, investigations of drug PK/PD behaviors and spatial tissue distribution in spleen are still rarely investigated [49]. Initially, TCC correlation analysis was performed, showing a significant correlation between MALDI MSI and LC-MS/MS measurements. As shown by H&E staining (Figure 6), three major functional zones of the spleen are tunica serosa, the hematogenous red pulp and the lymphoid white pulp [50]. The ion images suggest that tetrandrine can penetrate tunica serosa and accumulate in red and white pulp regions, and concentrations continue to increase until 240 min with no indication of decrease. In previous studies, the T_{max} of tetrandrine occurred at 4.5 h post-dose in spleen longer than those in other tissues, and the uptake efficiency of tetrandrine were higher in spleen than other tissues [38]. Tetrandrine was proved to increase prostaglandin E2 (PGE2) secretion in mesenchymal stem cells. It may likely activate the secretion of PGE2 in spleen resulting in inflammation and other side effects. On the other hand, it may be developed as a potent immunosuppressive agent targeting spleen [51].

Heart

Investigation of heart-specific spatio-temporal distribution is important to assess its potential cardiovascular side effects. MALDI MSI and LC-MS/MS measurements of TCC reveal a similar trend of tetrandrine in heart (Figure 2). Previous studies showed that the half-life ($t_{1/2}$) of tetrandrine in blood and heart was generally similar after *i.v.* administration, and rapidly excreted from heart [38]. In Figure 7A, the most abundant drug was distributed in the apex region at 10 min and 30 min time points. Similarly, we performed LC-MS/MS analysis of homogenates of different parts of heart tissues (Figure 7B) and MALDI imaging at 100 μm (Figure S7) to confirm the heterogeneous distribution of tetrandrine in heart. Samples collected at 10 min after drug administration were selected as representative tissue samples for validation. Results of LC-MS/MS analysis were consistent with MALDI imaging. That is, the relative amount of tetrandrine was significantly higher at the apex region compared to the rest of heart regions. Additionally, the ion images obtained at 400 μm (Figure 7A) and 100 μm (Figure S7) show a similar distribution pattern, confirming the heterogeneous distribution pattern of tetrandrine in

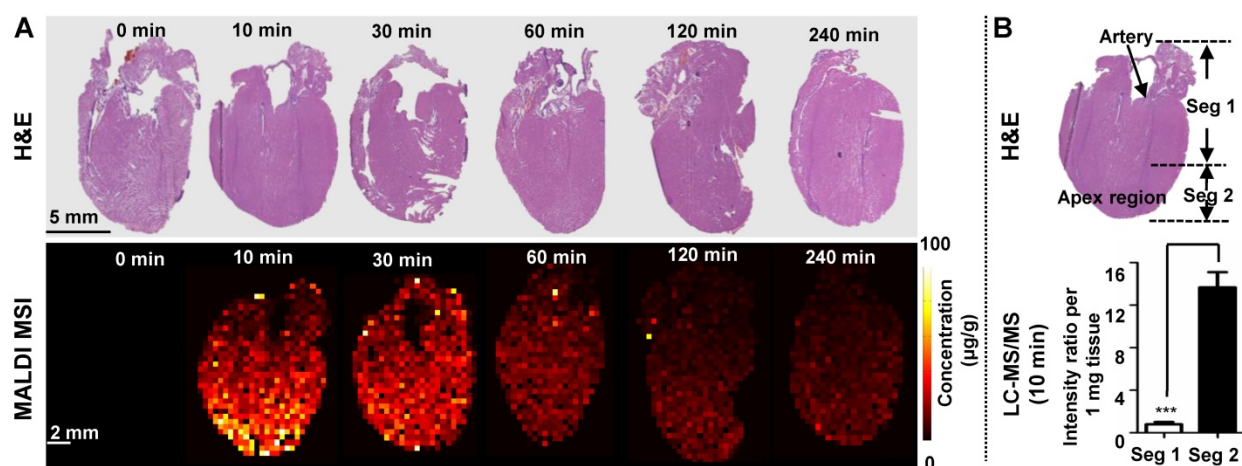


Figure 7. (A) MALDI MS imaging analysis of the tetrandrine distribution in heart tissues after *i.v.* administration. H&E staining of tissue sections obtained at different time points (top) and MALDI images represent the spatio-temporal distribution of tetrandrine across heart tissue sections (bottom). (B) Comparison of tetrandrine in heart tissues between the Seg 1 and 2 quantified using LC-MS/MS. The results were expressed as the mean \pm SD from three independent animals. Student's t-test was used for comparing two groups. *, significantly different between two groups at $p < 0.05$; **, $p < 0.01$ and ***, $p < 0.001$; n.s. as no significant difference between two groups.

heart tissues. Tetrandrine has been demonstrated as an ion channel blocker with high binding affinity to calcium channels (Ca^{2+}) [52]. Previous studies demonstrated that CaV1.2 was expressed in both the atria and ventricles of rat heart, however, the CaV1.2 message is more abundant in ventricle than in atria [53]. Therefore, heterogeneous distribution of tetrandrine in rat heart visualized by MALDI MS imaging may be correlated with the tissue-specific distribution of calcium channels. Additionally, although heart can be a potential tetrandrine targeting organ, the compound might require chemical structure modification to improve the bioavailability and enhance the effect of the drug with a single dose.

Conclusions

Many pharmacological properties of tetrandrine have been extensively investigated, whereas spatio-temporal distribution of tetrandrine is seldom interrogated. In this study, tetrandrine was quantitatively imaged in multiple rat organs with MALDI MS imaging. Normalizing drug ion signal against an appropriate internal standard is a straightforward method to compensate for ion suppression, matrix effects, and variances in tissue morphology. Furthermore, the developed quantitative MSI results were validated by quantitative LC-MS/MS, which showed a strong correlation between measurements from two methods.

Plasma levels of the drug and its metabolites often provide discrepant information on drug exposure at target organs and are not always sufficient for accurate interpretation and understanding of drug penetration, accumulation and elimination from organs. In this work, only lung and heart TCC show a similar trend as measured blood

TCC. Therefore, the spatially resolved drug quantitation acquired by MALDI MSI in lung, liver, kidney, spleen, and heart can provide significant information complementary to that acquired by traditional LC-MS/MS of tissue homogenates and WBA methods. With MSI results we can investigate further how tetrandrine exert its desired activity in target tissues and possibly overcome the shortcomings of tetrandrine such as poor bioavailability by chemical structure modifications, and enhance the effectiveness for the treatment of silicosis, hypertension, inflammation and lung cancer.

Abbreviations

MALDI MSI: matrix-assisted laser desorption/ionization mass spectrometry imaging; LC-MS/MS: liquid chromatography coupled with tandem mass spectrometry; WBA: whole-body autoradiography; PK: pharmacokinetics; PD: pharmacodynamics; ADME: adsorption, distribution, metabolism, and elimination; DHB: 2,5-dihydroxybenzoic acid; CHCA: α -cyano-4-hydroxycinnamic acid; *i.v.*: intravenous; IS: internal standard; ITO: indium tin oxide; ROI: region of interest; LLOQ: lower limit of quantification; TCC: time-concentration curve; $t_{1/2}$: half-life; T_{max} : time of maximum concentration; 3D: three-dimension.

Supplementary Material

Supplementary figures and table.

<http://www.thno.org/v09p0932s1.pdf>

Acknowledgments

This work was supported by the National Natural Science Foundation of China (No. 81773873, No. 81773887 and No. 81421005) and the 111 Project (No. B16046). The content is solely the responsibility

of the authors and does not necessarily represent the official views of the funding agencies.

Competing Interests

The authors have declared that no competing interest exists.

References

- Prideaux B, Via LE, Zimmerman MD, Eum S, Sarathy J, O'Brien P, et al. The association between sterilizing activity and drug distribution into tuberculosis lesions. *Nat Med*. 2015; 21: 1223-7.
- Prideaux B, Stoeckli M. Mass spectrometry imaging for drug distribution studies. *J Proteomics*. 2012; 75: 4999-5013.
- Andrew B McEwen CMH, Stuart G Wood. Quantitative whole-body autoradiography, LC-MS/MS and MALDI for drug-distribution studies in biological samples: the ultimate matrix trilogy. *Bioanalysis*. 2014; 6: 377-91.
- Solon EG. Autoradiography techniques and quantification of drug distribution. *Cell Tissue Res*. 2015; 360: 87-107.
- Penner N, Xu L, Prakash C. Radiolabeled absorption, distribution, metabolism, and excretion studies in drug development: why, when, and how? *Chem Res Toxicol*. 2012; 25: 513-31.
- Andrew McEwen CH. Quantitative whole-body autoradiography: past, present and future. *Bioanalysis*. 2015; 7: 557-68.
- Li B, Neumann EK, Ge J, Gao W, Yang H, Li P, et al. Interrogation of spatial metabolome of Ginkgo biloba with high-resolution matrix-assisted laser desorption/ionization and laser desorption/ionization mass spectrometry imaging. *Plant Cell Environ*. 2018.
- Li B, Dunham SJB, Ellis JF, Lange JD, Smith JR, Yang N, et al. A Versatile Strategy for Characterization and Imaging of Drip Flow Microbial Biofilms. *Anal Chem*. 2018; 90: 6725-34.
- Kompauer M, Heiles S, Spengler B. Atmospheric pressure MALDI mass spectrometry imaging of tissues and cells at 1.4- μm lateral resolution. *Nat Methods*. 2017; 14: 90-6.
- Rubakhin SS, Romanova EV, Nemes P, Sweedler JV. Profiling metabolites and peptides in single cells. *Nat Methods*. 2011; 8: S20-9.
- Wang X, Han J, Hardie DB, Yang J, Pan J, Borchers CH. Metabolomic profiling of prostate cancer by matrix assisted laser desorption/ionization-Fourier transform ion cyclotron resonance mass spectrometry imaging using Matrix Coating Assisted by an Electric Field (MCAEF). *Biochim Biophys Acta Proteins Proteom*. 2017; 1865: 755-67.
- Chughtai K HRMA. Mass spectrometric imaging for biomedical tissue analysis. *Chem Rev*. 2010; 110: 3237-77.
- Baker TC, Han J, Borchers CH. Recent advancements in matrix-assisted laser desorption/ionization mass spectrometry imaging. *Curr Opin Biotechnol*. 2017; 43: 62-9.
- Solon EG, Schweitzer A, Stoeckli M, Prideaux B. Autoradiography, MALDI-MS, and SIMS-MS imaging in pharmaceutical discovery and development. *AAPS J*. 2010; 12: 11-26.
- Chen X, Hatis P, Judge J, Argikar UA, Ren X, Sarber J, et al. Compound Property Optimization in Drug Discovery Using Quantitative Surface Sampling Micro Liquid Chromatography with Tandem Mass Spectrometry. *Anal Chem*. 2016; 88: 11813-20.
- Fonville JM, Carter C, Cloarec O, Nicholson JK, Lindon JC, Bunch J, et al. Robust data processing and normalization strategy for MALDI mass spectrometric imaging. *Anal Chem*. 2012; 84: 1310-9.
- Takai N, Tanaka Y, Inazawa K, Saji H. Quantitative analysis of pharmaceutical drug distribution in multiple organs by imaging mass spectrometry. *Rapid Commun Mass Spectrom*. 2012; 26: 1549-56.
- Pirman DA, Kiss A, Heeren RM, Yost RA. Identifying tissue-specific signal variation in MALDI mass spectrometric imaging by use of an internal standard. *Anal Chem*. 2013; 85: 1090-6.
- Hamm G, Bonnel D, Legouffe R, Pamelard F, Delbos JM, Bouzom F, et al. Quantitative mass spectrometry imaging of propranolol and olanzapine using tissue extinction calculation as normalization factor. *J Proteomics*. 2012; 75: 4952-61.
- Groseclose MR, Castellino S. A mimetic tissue model for the quantification of drug distributions by MALDI imaging mass spectrometry. *Anal Chem*. 2013; 85: 10099-106.
- Clemis EJ, Smith DS, Camenzind AG, Danell RM, Parker CE, Borchers CH. Quantitation of spatially-localized proteins in tissue samples using MALDI-MRM imaging. *Anal Chem*. 2012; 84: 3514-22.
- Kallback P, Nilsson A, Shariatgorji M, Andren PE. msiQuant—Quantitation Software for Mass Spectrometry Imaging Enabling Fast Access, Visualization, and Analysis of Large Data Sets. *Anal Chem*. 2016; 88: 4346-53.
- Robichaud G, Garrard KP, Barry JA, Muddiman DC. MSiReader: an open-source interface to view and analyze high resolving power MS imaging files on Matlab platform. *J Am Soc Mass Spectrom*. 2013; 24: 718-21.
- Yu X, Changqi Zou, Mubin Lin. Observation of the effect of tetrandrine on experimental silicosis of rats. *Ecotox Environ Safety*. 1983; 7: 306-12.
- Shen DF, Tang QZ, Yan L, Zhang Y, Zhu LH, Wang L, et al. Tetrandrine blocks cardiac hypertrophy by disrupting reactive oxygen species-dependent ERK1/2 signalling. *Br J Pharmacol*. 2010; 159: 970-81.
- Wan J, Liu T, Mei L, Li J, Gong K, Yu C, et al. Synergistic antitumor activity of sorafenib in combination with tetrandrine is mediated by reactive oxygen species (ROS)/Akt signaling. *Br J Cancer*. 2013; 109: 342-50.
- Song N, Zhang S, Li Q, Liu C. Establishment of a liquid chromatographic/mass spectrometry method for quantification of tetrandrine in rat plasma and its application to pharmacokinetic study. *J Pharm Biomed Anal*. 2008; 48: 974-9.
- Jin H, Li L, Zhong D, Liu J, Chen X, Zheng J. Pulmonary toxicity and metabolic activation of tetrandrine in CD-1 mice. *Chem Res Toxicol*. 2011; 24: 2142-52.
- Qi XM, Miao LL, Cai Y, Gong LK, Ren J. ROS generated by CYP450, especially CYP2E1, mediate mitochondrial dysfunction induced by tetrandrine in rat hepatocytes. *Acta Pharmacol Sin*. 2013; 34: 1229-36.
- Wang N, Pan W, Zhu M, Zhang M, Hao X, Liang G, et al. Fangchinoline induces autophagic cell death via p53/sestrin2/AMPK signalling in human hepatocellular carcinoma cells. *Br J Pharmacol*. 2011; 164: 731-42.
- Yuan SY, Yang CR, Cheng CL, Hsu SL, Liao JW, Lin CC, et al. Comparative nephrotoxicity of aristolochic acid and tetrandrine in vitro and in vivo. *Int J Toxicol*. 2011; 30: 35-46.
- Guo S, Wang Y, Zhou D, Li Z. Electric Field-Assisted Matrix Coating Method Enhances the Detection of Small Molecule Metabolites for Mass Spectrometry Imaging. *Anal Chem*. 2015; 87: 5860-5.
- Pirman DA, Yost RA. Quantitative tandem mass spectrometric imaging of endogenous acetyl-L-carnitine from piglet brain tissue using an internal standard. *Anal Chem*. 2011; 83: 8575-81.
- Chumbley CW, Reyzer ML, Allen JL, Marriner GA, Via LE, Barry CE, 3rd, et al. Absolute Quantitative MALDI Imaging Mass Spectrometry: A Case of Rifampicin in Liver Tissues. *Anal Chem*. 2016; 88: 2392-8.
- Li D, Cao Z, Liao X, Yang P, Liu L. The development of a quantitative and qualitative method based on UHPLC-QTOF MS/MS for evaluation paclitaxel-tetrandrine interaction and its application to a pharmacokinetic study. *Talanta*. 2016; 160: 256-67.
- Tsai J J MJKH, Wang T F, Wang S R, Kao D H, . The Modulatory effect of tetrandrine on the CD23, CD25 and HLA-DR expression and cytokine production in different groups of asthmatic patients. *Int Arch Allergy Immunol*. 1995; 108: 183-8.
- Wang H L ZXH, Hong Y, Jin X, Xing J, Jin H Y, Liu X J, Zhang D R. Tetrandrine prevents monocrotaline-induced pulmonary hypertension in rats. *Drug Develop Res*. 1996; 39: 158-60.
- Aixia J, QiuHong L. Pharmacokinetics, tissue distribution and excretion study of tetrandrine in rats. *Journal of Chinese Pharmaceutical Sciences*. 2015; 24.
- Nunn JF. Applied respiratory physiology. Oxford, UK: Butterworth-Heinemann; 2013.
- Shi JP, Li SX, Ma ZL, Gao AL, Song YJ, Zhang H. Acute and sub-chronic toxicity of tetrandrine in intravenously exposed female BALB/c mice. *Chin J Integr Med*. 2016; 22: 925-31.
- Tian Y, Shen S, Jiang Y, Shen Q, Zeng S, Zheng J. CYP3A5 mediates bioactivation and cytotoxicity of tetrandrine. *Arch Toxicol*. 2016; 90: 1737-48.
- Asha S, Vidyavathi M. Role of human liver microsomes in vitro metabolism of drugs—a review. *Appl Biochem Biotechnol*. 2010; 160: 1699-722.
- Ronci M, Rudd D, Guinan T, Benkendorff K, Voelcker NH. Mass spectrometry imaging on porous silicon: investigating the distribution of bioactives in marine mollusc tissues. *Anal Chem*. 2012; 84: 8996-9001.
- Gustafsson OJR, Guinan TM, Rudd D, Kobus H, Benkendorff K, Voelcker NH. Metabolite mapping by consecutive nanostructure and silver-assisted mass spectrometry imaging on tissue sections. *Rapid Commun Mass Spectrom*. 2017; 31: 991-1000.
- Rudd D, Ronci M, Johnston MR, Guinan T, Voelcker NH, Benkendorff K. Mass spectrometry imaging reveals new biological roles for choline esters and Tyrian purple precursors in muricid molluscs. *Sci Rep*. 2015; 5: 13408.
- Choi HS KH, Min KR, Kim Y, Lim HK, Chang YK, Chung MW. Anti-inflammatory effects of fangchinoline and tetrandrine. *J Ethnopharmacol*. 2000; 69: 173-9.
- Koh SB BJ, Lee BY, Seong YH. Protective Effects of Fangchinoline and Tetrandrine on Hydrogen Peroxide-Induced Oxidative Neuronal Cell Damage in Cultured Rat Cerebellar Granule Cells. *Planta Med*. 2003; 69: 506-12.
- Li D, Liu H, Liu Y, Zhang Q, Liu C, Zhao S, et al. Design, synthesis and biological activities of tetrandrine and fangchinoline derivatives as antitumor agents. *Bioorg Med Chem Lett*. 2017; 27: 533-6.
- Cataldi M, Vigliotti C, Mosca T, Cammarota M, Capone D. Emerging Role of the Spleen in the Pharmacokinetics of Monoclonal Antibodies, Nanoparticles and Exosomes. *Int J Mol Sci*. 2017; 18.
- Pislyagin EA, Dmitrenok PS, Gorpenchenko TY, Avilov SA, Silchenko AS, Aminin DL. Determination of cucumarioside A(2)-2 in mouse spleen by radiopectroscopy, MALDI-MS and MALDI-IMS. *Eur J Pharm Sci*. 2013; 49: 461-7.
- Yang Z, Concannon J, Ng KS, Seyb K, Mortensen LJ, Ranganath S, et al. Tetrandrine identified in a small molecule screen to activate mesenchymal stem cells for enhanced immunomodulation. *Sci Rep*. 2016; 6: 30263.
- Gang Wang JRL, Costantino Iadecola. Herbal alkaloid tetrandrine: from an ion channel blocker to inhibitor of tumor proliferation. *Trends Pharmacol Sci*. 2004; 25: 120-3.

53. Larsen JK, Mitchell JW, Best PM. Quantitative analysis of the expression and distribution of calcium channel alpha 1 subunit mRNA in the atria and ventricles of the rat heart. *J Mol Cell Cardiol.* 2002; 34: 519-32.